Proceedings of the 20th International Conference on Soil Mechanics and Geotechnical Engineering– Rahman and Jaksa (Eds)

Examining the initiation mechanisms of earthquake-induced flow failure of tailings impoundments using centrifuge shaking table tests

Examen des mécanismes d'amorçage de la rupture d'écoulement induite par un séisme dans les bassins de retenue des résidus à l'aide d'essais sur table à secousses centrifuges

Zitao Zhang, Jing Hu, Xuedong Zhang & Jianhui Liang

State Key Laboratory of Simulation and Regulation of Water Cycle in River Basin, China Institute of Water Resources and Hydropower Research, Beijing, 100038, China, zhangzt@iwhr.com.

ABSTRACT: In this study, centrifuge shaking table tests were conducted to characterize the failure mechanisms of tailings impoundments subjected to seismic sequences. The ejection of tailings, mudflows along the downstream slope of the starter dam and the topographic features observed in real tailings impoundments after earthquake-induced failure are reproduced in the tests. The experimental results indicate that the initial earthquakes may only lead to localized deformation near the silty layers at shallow depths, followed by lateral spreading of tailings between the silty layers at deeper locations. The continuous buildup of excess pore pressure may lead to ejection of tailings during the subsequent earthquakes. After that, dissipation of excess pore pressure occurs in the upstream side, while the tailings near slope crest become liquefied and flow along the slope surface. The slope profile keeps changing with increasing the number of loading cycles until an extremely gentle slope with an angle of 1-2° emerges at the upper surface of the tailings. Afterwards, the tailings at extremely shallow depths seem to be liquefied and then flow toward the downstream direction layer by layer, leading to the release of tailings. In addition, due to the continuous lateral spreading or sliding of tailings at deeper locations towards the downstream direction, the tailings eventually flow along the slope surface and then are released, which contributes to a significant increase in the release rate. The salient findings can shed light on the associated failure mechanisms and then improve the seismic design of tailings impoundments, and the unique and invaluable observations can also be used to validate constitutive models, procedures and results of numerical methods.

RÉSUMÉ : Dans cette étude, des essais sur table à secousses centrifuges ont été menés pour caractériser les mécanismes de défaillance des parcs à résidus soumis à des séquences sismiques. L'éjection des résidus, les coulées de boue le long de la pente en aval du barrage de démarrage et les caractéristiques topographiques observées dans les bassins de résidus réels après une rupture induite par un séisme sont reproduites dans les essais. Les résultats expérimentaux indiquent que les séismes initiaux ne peuvent conduire qu'à une déformation localisée près des couches limoneuses à faible profondeur, suivie d'un étalement latéral des résidus entre les couches limoneuses à des endroits plus profonds. L'accumulation continue d'une pression interstitielle excessive peut conduire à l'éjection de résidus au cours des tremblements de terre ultérieurs. Après cela, la dissipation de la pression interstitielle excessive se produit du côté amont, tandis que les résidus près de la crête de la pente se liquéfient et s'écoulent le long de la surface de la pente. Le profil de la pente ne cesse de changer avec l'augmentation du nombre de cycles de chargement jusqu'à ce qu'une pente extrêmement douce avec un angle de 1-2° émerge à la surface supérieure des résidus. Par la suite, les résidus à des profondeurs extrêmement faibles semblent se liquéfier puis s'écouler vers l'aval couche par couche, entraînant le relâchement des résidus. De plus, en raison de l'étalement ou du glissement latéral continu des résidus à des endroits plus profonds vers l'aval, les résidus finissent par s'écouler le long de la surface de la pente puis sont libérés, ce qui contribue à une augmentation significative du taux de libération. Les résultats saillants peuvent faire la lumière sur les mécanismes de défaillance associés, puis améliorer la conception sismique des bassins de résidus, et les observations uniques et inestimables peuvent également être utilisées pour valider les modèles constitutifs, les procédures et les résultats des méthodes numériques.

KEYWORDS: Failure mechanisms, earthquake sequences, tailings impoundments, centrifuge shaking table tests, release of tailings.

1 INTRODUCTION

Billions of tonnes of tailings are annually produced across the globe by the extractive mining industry (Fyfe 1981; Adiansyah et al. 2015; Owen et al. 2020). Storage of these produced tailings in dammed impoundments is currently one of the main methods to handle those tailings (Lottermoser 2007; Kossoff et al. 2014). The failures of tailings impoundments can result in high-velocity long-runout mudflows, leading to immediate fatalities and direct economic losses. Moreover, the harmful emplaced materials can contaminate soils, river sediments, floodplains, riverbanks and water, thus causing long-term impacts on human health and the environment (Hatje et al. 2017; Vergilio et al. 2020; Dong et al. 2020). As summarized by Santamarina et al. (2019), nearly 3000 people have been killed and nearly 270 Mm^3 of tailings have been released in the associated failure events over the past century. It is therefore of great importance to examine the underlying failure mechanisms of tailings impoundments.

Seismic loading is one of the main triggers of tailings impoundment failures (Villavicencio et al. 2014). The most disastrous failure occurred at El Cobre N° 1 dam, Chile, as a result of the 1965 La Ligua earthquake (7.5 Richter magnitude), the epicenter of which was 68 km away from the dam. An enormous volume of tailings (1.9 million m^3) has been released after dam breach. The run-out distance of the mud-flow reached 12 km, and the flow velocity was estimated to be as high as 20 km/h; this caused an enormous destruction of a town in the flow path and killed about 300 people (Dobry and Alvares 1967; Blight and Fourie 2005). Failure of the tailings impoundments may also occur during the aftershocks following a mainshock or during earthquake swarms, i.e., sequences of small or moderate magnitude earthquakes that occur in a relatively short period without a specific mainshock (Tanner et al. 2020). As pointed out by Agurto-Detzel et al. (2016), the small-magnitude seismic sequence might have contributed to the failure of the Samarco tailings dam in Brazil. The 1966 Matsushiro earthquake swarms

(Central Honshu, Japan) with an activity of up to ~7000 small earthquakes per day lead to ground fissures, spring water and numerous landslides (Zobin 2017). As the majority of the associated studies only consider a main shock and do not account for a seismic sequence (Khanal and Saygili 2019), the failure mechanisms of tailings impoundments subjected to seismic sequences remain unclear.

This study aims to characterize the failure mechanisms of upstream tailings impoundments subjected to seismic sequences by centrifuge shaking table tests. The centrifuge tests are more efficient and advantageous than 1g tests as the in situ stress field and soil properties can be reproduced in the centrifuge (Kim et al. 2011; Madabhushi et al. 2018; Shi et al. 2019; Zhang et al. 2019). The experimental details are presented first, followed by experimental results and discussions regarding soil deformation and the pore pressure evolutions. The focus is put on how the tailings impoundments deform and eventually lead to the release of tailings under earthquake sequences. The salient findings can shed light on the associated failure mechanisms and then improve the seismic design of tailings impoundments. The unique and invaluable observations can also be used to validate constitutive models, procedures and results of numerical methods.

2 EXPERIMENTAL DETAILS

The model tests were conducted at the China Institute of Water Resources and Hydropower Research (IWHR) by a horizontal-vertical centrifuge shaking table installed on a beam centrifuge with a capacity of 450 g-ton and a radius of 5.03 m. The centrifuge shaking table can operate up to 100g with a payload mass of up to 440 kg. It can simultaneously simulate horizontal and vertical bedrock motions with peak accelerations of up to 30g and 20g at model scale, respectively. This study only used horizontal dynamic excitation and the centrifugal acceleration was set to 40g, i.e., $N = 40$. As summarized in Table 1, the scaling factors follow the well-established scaling laws for centrifuge shaking table tests (Schofield 1981). In order to avoid the time scaling conflict for consolidation and for the seismic motion, the viscosity of the pore fluid was increased 40-fold by using an aqueous solution of hydroxypropyl methylcellulose (HPMC), which is commonly used in centrifuge shaking table tests (e.g., Stewart 1998).

Table 1. Scaling factors used in the centrifuge shaking table tests carried out at *N*g.

Item	Scaling factor (model/prototype)
Length	1/*N*
Time	1/*N*
Acceleration	*N*
Frequency	*N*
Displacement	1/*N*
Coefficient of viscosity	*N*

2.1 *Model configuration*

Fig. 1 shows the centrifuge model of tailings impoundment. The model was prepared in a rigid container with inner dimensions of 0.9 m (length) × 0.2 m (width) × 0.5 m (height), which was equipped with a transparent perspex side window to facilitate the image-based analysis. The model was mainly composed of a starter dam with a height of 160 mm and a slope ratio of 1:1.5 (height : width) and a slope of tailings with a height of 260 mm and a slope ratio of 1:3. The slope ratio is frequently used in the tailings impoundments both in China (Chen et al. 2007) and the rest of the world (Villavicencio et al. 2014; Ishihara et al. 2015). Since sub-dams had relatively small sizes compared with the whole tailings impoundments, they were not separately constructed in the model to facilitate preparation, which had also been used in previous model tests (e.g., Jin et al. 2018). This treatment has a minor effect on the seismic failure mechanisms of tailings impoundments.

As shown in Fig. 1, the tailings impoundment had a laminar structure. Two silty layers were sandwiched in the tailings slope at heights of 230 mm and 180 mm, i.e., at 88% and 69% of the total model height, respectively. This treatment is used to roughly simulate the stratigraphic properties of real tailings impoundments, e.g., the Mochikoshi tailings impoundment in Japan (Ishihara 1984) and the Lixingou tailings impoundment in China (Zhang 2006), where the soil profiles are characterized by sandy tailings with weakly permeable silty interlayers. The formation of this horizontal laminar structure can be attributed to the sedimentation process of tailings. As indicated by the results of field investigations, such a layered structure or stratification also exists in the sand deposits that experienced similar sedimentation processes, e.g., natural fluvial ground at the mouth of rivers and reclaimed ground formed by hydraulic filling (Kokusho and Kojima 2002).

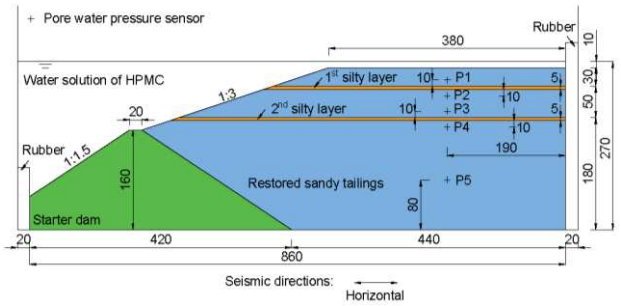

Figure 1. Schematic drawing of the centrifuge model of tailings impoundment.

2.2 *Model preparation*

The starter dam was firstly prepared. Since typical starter dams were usually constructed using natural soils and rock-fills, the model material were chosen as coarse silica sand with particle sizes of 2-4 mm produced in Fujian Province, China. The dry sand was firstly placed to form a level-ground and then was compacted layer by layer in the container until the dry density reached 1.9 g/cm^3, which was close to the value used in practice. When the thickness of the sands reached 160 mm, a careful excavation was conducted to expose the geometry of the starter dam.

After constructing the starter dam, the dry tailings slope was prepared using tailings collected from a real tailings impoundment of a gold mine in Gansu Province, China. The material was categorized as silty sand and had a maximum size of 0.1 mm and contained 31.2% of fines with sizes smaller than 0.075 mm. The maximum dry density was 1.592 g/cm^3, while the minimum dry density was 1.136 g/cm^3. The air pluviation method was used to prepare the tailings slope, and the achieved dry density was 1.40 g/cm^3, corresponding to a relative density of 66% after sample preparation. With regard to the silty layers, silts were gently placed on the surface of the tailings at the prescribed elevation to form a layer with a thickness of 5 mm, and the achieved density was 1.44 g/cm^3. The effective particle size d_{10} was 1~10μm, which was close to the field value (e.g., Ishihara 1984). As the hydraulic conductivity is mainly determined by d_{10}, this ensures the similarity of soil properties of prototype and model silty layers.

Since the phreatic surface was only slightly lower than the slope surface in practice and the tailings in the impoundments were nearly fully saturated (Ishihara et al. 2015), the centrifuge model was immersed in liquid to maintain the saturation condition during the spin-up of the centrifuge and the subsequent shaking process.

2.3 *Instrumentation layout*

As shown in Fig. 1, a series of vertically distributed miniature pore pressure sensors were installed at various depths in the upstream part to monitor the generation and dissipation of pore pressure. In addition, two high-speed cameras (Model: Hero 8, GoPro Inc., USA) and particle image velocimetry (PIV) techniques were used to capture the displacement field. The spin-up process was monitored at a frame rate of 30 fps and a resolution of 4000 × 3000 pixels, while a frame rate of 240 fps and a resolution of 1280 × 960 pixels were used to monitor the shaking process. Since the texture of tailings could hardly be identified, silica fume (with a size of 48 μm) was used to prepare the trace markers distributed at several horizontally distributed arrays to visualize motion. As shown in Fig. 2, a coordinate system is used to indicate the initial locations of trace markers. The origin is put at the initial slope crest, while x_0 and z_0 denote horizontal and vertical distances from the origin to a particular point. The discussions on soil deformation are mainly based on the results of array 1 near upper surface and arrays 2 and 3 between the two silty layers. The average values of z_0, i.e., initial depths of array 1, 2 and 3 are 4 mm, 40 mm and 60 mm, respectively.

2.4 *Experimental procedures*

The dry model was saturated under vacuum using an aqueous solution of HPMC in a saturation box. The mass flux of the aqueous solution was controlled to as low as 0.3-0.4 kg/h using a peristaltic pump to prevent fluidization of the materials. Then, the model was mounted on the surface of the centrifuge shaking table. After completing all these preparation steps, the centrifuge started to spin-up and the centrifugal acceleration gradually increased to 40*g*. The model was then subjected to horizontal seismic motions after a specific time of stabilization. As shown in Fig. 1, the shaking direction was along the longitudinal direction of the container and was perpendicular to the dam axis.

The total duration of the seismic sequence was 120 s, corresponding to 80 min at prototype scale. The peak acceleration in each cycle was 1-7.2*g* at model scale, corresponding to 0.025-0.18*g* at prototype scale. The input motion had high frequency components at 36 Hz, corresponding to 0.9 Hz at prototype scale. The total number of loading cycles was estimated to be in the range of 4000-5000. Therefore, the model was subjected to a seismic sequence of hundreds of small-magnitude earthquakes in a relatively short period, which roughly simulated the real earthquake sequences (e.g., Zobin 2017; Tanner et al. 2020).

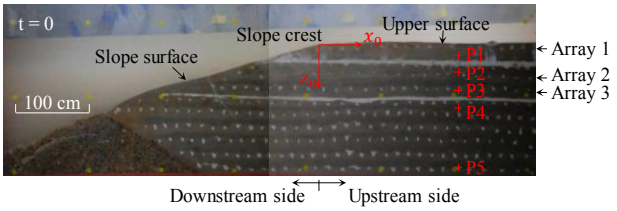

Figure 2. Picture of the tailings impoundment model before shaking.

3 RESULTS AND DISCUSSION

Fig. 3 presents the slope conditions after shaking at t = 120 s, where t denotes time in model scale. The sandy tailings slope with silty interlayers failed, leading to a massive release of tailings. The volume of released tailings is estimated to be about 20% of the total volume of those tailings initially located above the crest of the starter dam. Due to such a release, the height of the tailings impoundment is reduced to about 83% of its initial value. The key features observed during shaking are further elaborated in the following. It is worth noting that all results are presented in model units unless otherwise indicated.

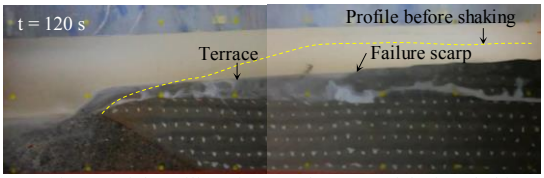

Figure 3. Picture of the tailings impoundment model after shaking at t = 120 s.

3.1 *Ejection of tailings and dissipation of excess pore pressure*

For a sandy tailings slope with a laminar structure, the initial earthquakes only lead to localized deformation near the silty layers at shallow depths, followed by lateral spreading of tailings between the silty layers at deeper locations. Those localized deformations can be attributed to the rapid buildup of pore pressure under silty layers (see Fig. 4). Although detachment and translocation of tailings protrusions may occur at the slope surface, the overall deformation of the tailings slope and the release of tailings are limited.

The continuous buildup of pore pressure may lead to ejection of tailings during the subsequent earthquakes. As shown in Fig. 5, ejection of tailings or sand boiling occurs at x_0 = 250 mm, and lasts nearly 1 sec from 17 to 18 s. This suggests that the tailings directly below the silty layers might have reached the liquefaction state, and the liquefied tailings are prone to ejection onto the surface to form sand boils under the high hydraulic gradient. This is consistent with the fact that many sand volcanos have been observed at sites of earthquake-induced failures of tailings impoundments, e.g., Mochikoshi No. 1 dike in Japan (Ishihara 1984). In addition, as shown in Fig. 4, the excess pore pressure (Δu) turns to dissipate with increasing loading cycles in the upstream part. This indicates that the ejection of tailings might change the drainage conditions of the tailings and then influence the pore pressure evolution.

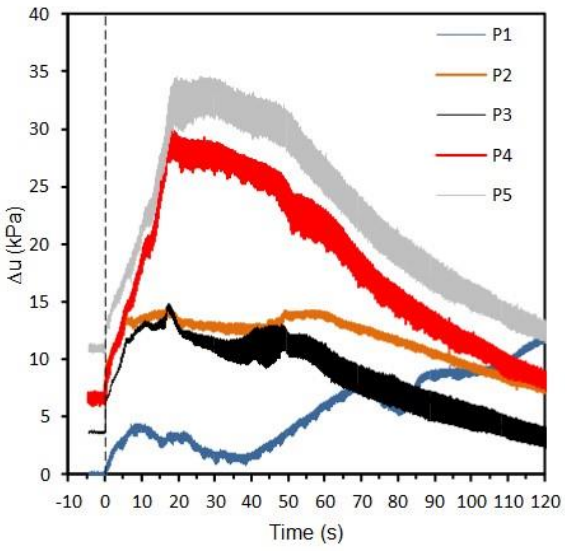

Figure 4. Evolutions of excess pore pressure (Δu) at different depths with time during shaking.

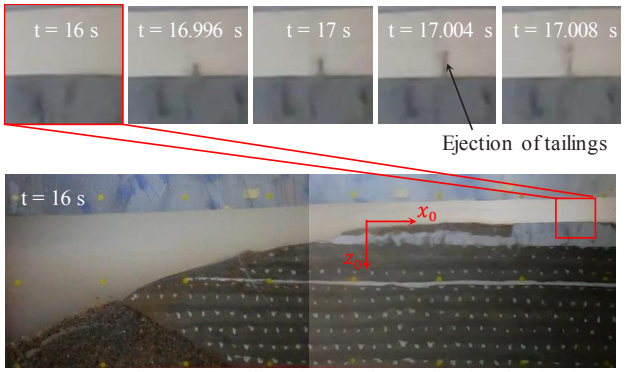

Figure 5. Snapshots of the tailings impoundment showing the ejection of tailings.

3.2 *Sliding of tailings above the second silty layer*

After ejection of tailings, the horizontal displacements (d_h) of trace markers far exceed the vertical displacements in arrays 2 and 3, and the maximum value of d_h is observed near slope surface, which follows the trend of lateral spreading observed before ejection. Fig. 6 presents evolutions of horizontal displacements of those trace markers. Since the particles in the silty layers may move upwards through the interface between tailings and the side window, thus hindering the identification of some of the trace markers. As indicated by the legend, those trace markers shown in Fig. 6 are located at x_0 = -144 to -12 mm in the downstream side and at x_0 = 201-256 mm in the upstream side. The trace markers in the downstream side move toward the downstream direction in a larger speed after ejection of tailings. The horizontal displacements of all the trace markers located in the downstream side reach 20 mm at model scale or 0.8 m at prototype scale after a duration of 40-50 s. With regard to the upstream side, the trace markers start to move toward the downstream direction after ejection, and then the values of d_h reach a plateau at about t = 25 s, suggesting that horizontal movement have already ceased in those tailings.

The relative displacements of those trace markers are further calculated to investigate soil deformations at different locations. The relative displacement in the downstream side is given by the difference between the displacement at x_0 = -144 mm and at x_0 = -12 mm, i.e., $d_{h,-144mm}$ - $d_{h,-12mm}$. As shown in Fig. 7, the relative displacement in the downstream side is only 0.5 mm at t = 35 s, and the value increases to 3.3 mm at t = 50 s. The difference between displacements at x_0 = -12 mm and x_0 = 201 mm, i.e., $d_{h,-12mm}$ - $d_{h,201mm}$, is used to reflect the relative displacement in the upstream side. The value continuously increases with time and reaches 14.4 mm at 50 s, which is much larger than that in the downstream side. This suggests that the tailings in the downstream side move as a whole and slide along a failure plane in the second silty layer or along the interface between the silty layer and tailings.

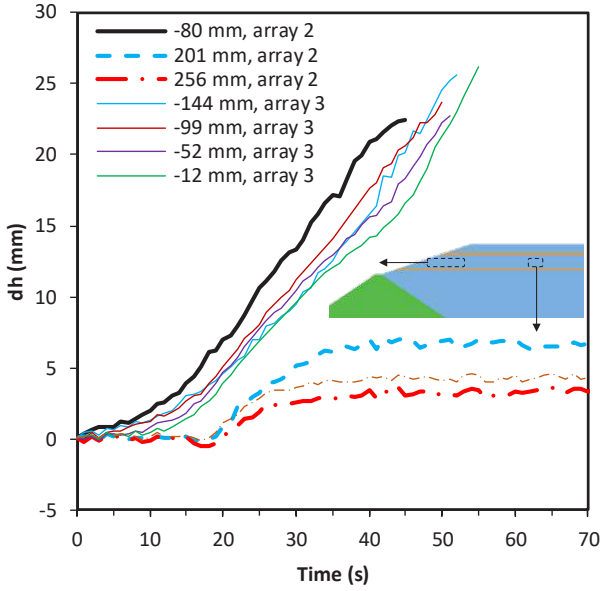

Figure 6. Evolutions of horizontal displacements of the trace markers in arrays 2 and 3 with time during shaking.

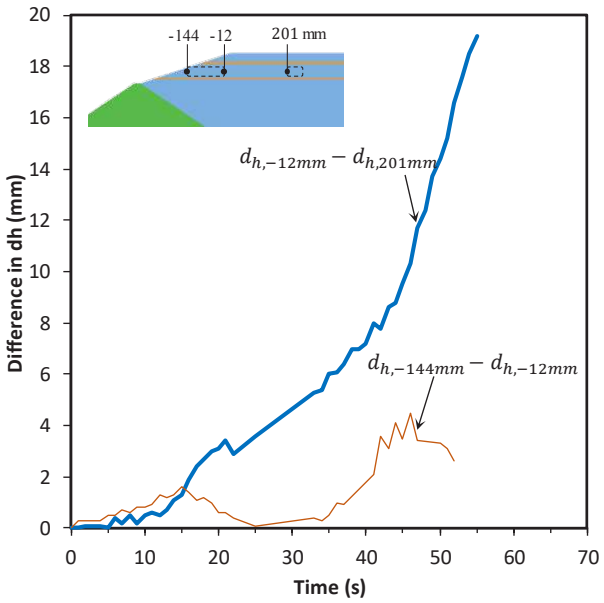

Figure 7. Evolutions of the relative displacements, i.e., $d_{h,-12mm}$-$d_{h,201mm}$ and $d_{h,-144mm}$-$d_{h,-12mm}$, with time during shaking.

3.3 *Liquefaction and flow of tailings at extremely shallow depths*

As shown in Fig. 8a, because of the extremely small confining stress at extremely shallow depths near the upper surface, tailings can be easily liquefied under seismic loading. Then, these tailings flow along the slope surface and the downstream slope of the starter dam, and eventually arrive at the deposition space between the slope of the starter dam and the side walls of the container. As the flow moves in extremely thin layers, it can hardly be clearly identified in the slope surface via the images. However, the accumulation of tailings in the deposition space clearly demonstrates the occurrence of tailings flow.

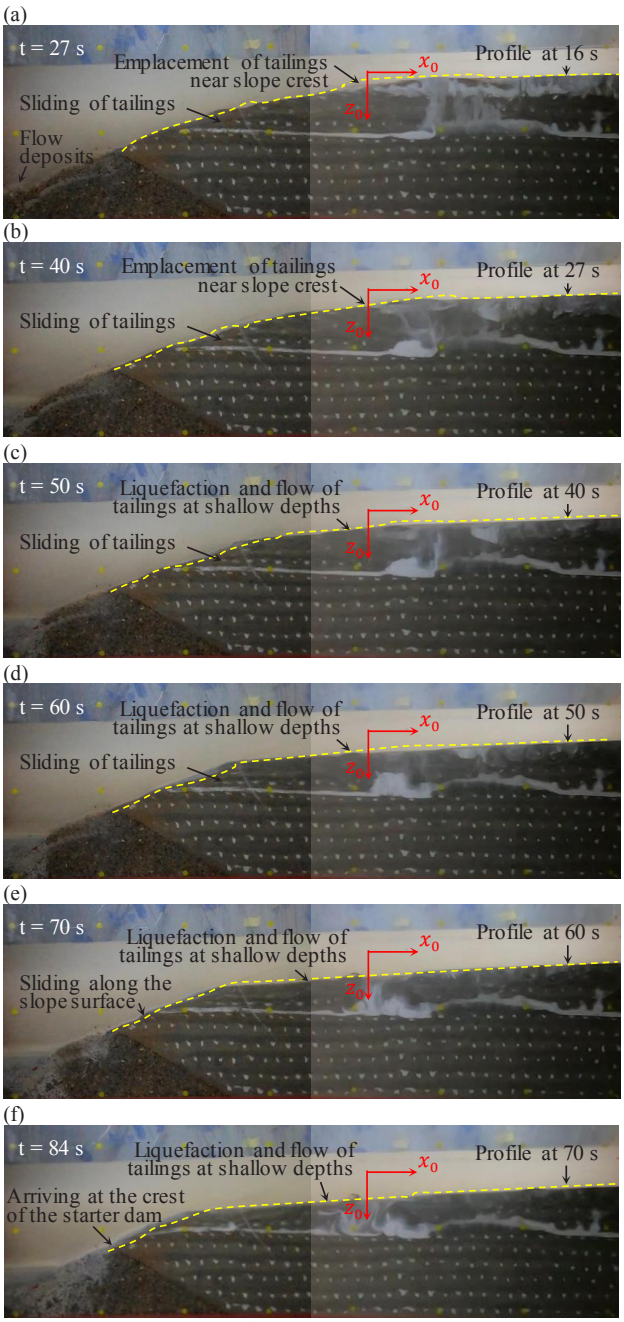

Figure 8. Snapshots of the tailings impoundment collected at (a) t = 27 s, (b) t = 40 s, (c) t = 50 s, (d) t = 60 s, (e) t = 70 s and (f) t = 84 s.

As shown in Figs. 8b and 8c, because of the continuous flow of the liquefied tailings at extremely shallow depths, the slope profile keeps changing with increasing time. An extremely gentle slope with an angle of 1-2° emerges at t = 50 s. Afterwards, as shown in Figs. 8d, 8e and 8f, the tailings at extremely shallow depths seem to be liquefied and then flow toward the downstream direction layer by layer. The height of the tailings impoundment continues to decrease because of the continuous flow of tailings. The collected images indicate that the model height at x_0 = 0 is decreased by 14% at t = 84 s, suggesting a significant release of tailings. Such behavior can also be assessed by the measurements from P1. The sensor P1, initially located at a depth of ~19 mm, might gradually emerge with the flow of upper tailings. Then, the value reflects the static liquid pressure at the current upper surface. As shown in Fig. 8, the pressure at P1 increases with time from 40 s to 70 s with a total increase of 6.2 kPa, which corresponds to a model height reduction of 16 mm, i.e., ~6% of the initial model height.

3.4 *Flow of tailings above the second silty layer*

Because of the continuous sliding of tailings as discussed in section 3.2, the downstream end of those tailings gradually moves downward and along the slope surface. As shown in Fig. 8f, those tailings arrive at the crest of the starter dam at t = 84 s, and then flow along the downstream slope of the starter dam, which is similar to the field observations (e.g., Ishihara 1984; Ishihara et al. 2015). As shown in Fig. 9a, not only the tailings at extremely shallow depths, but also those at larger depths above the second silty layer, flow toward the downstream direction along the slope surface. According to the deposition volume estimated via images, the flow rate can be roughly determined. The average flow rate from 60 s to 84 s was about 6.7 cm^3/s, while the average flow rate from 84 s to 120 s was about 16.7 cm^3/s, which is about 2.5-fold of the previous value. This suggests that the flow of tailings above the second silty layer contributes to a significant increase in the release rate of tailings.

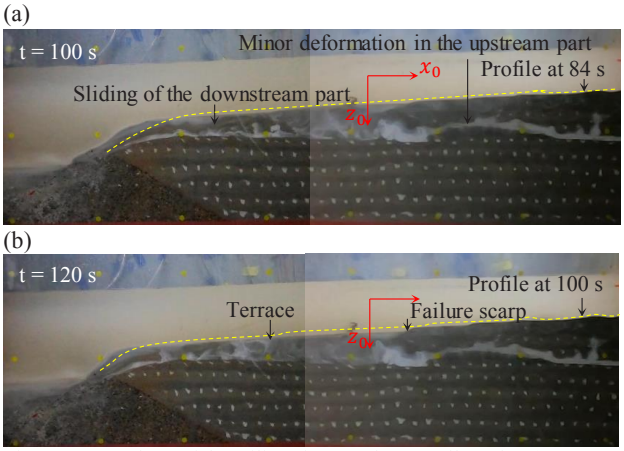

Figure 9. Snapshots of the tailings impoundment collected at (a) t = 100 s and (b) t = 120 s.

3.5 *Formation of terraces and scarps*

As shown in Fig. 9, the flow of tailings seems to have ceased in the upstream part, while the downstream part continues to spread laterally. The tailings left in place exhibit a failure scarp at x_0 = 50 mm and a 378-mm wide terrace at the downstream side at t = 120 s. Several small terraces and scarps can also be identified at the upstream side. This topographic feature is similar to that observed in real tailings impoundments after earthquake-induced failure, e.g., Barahona No. 1 dam, Chile (Troncoso et al. 1993) and El Cobre Viejo dam, Chile (Villavicencio et al. 2014; Blight and Fourie 2005). The failure mechanisms observed in this study can be used to explain this topographic feature. Due to the liquefaction and flow of tailings at extremely shallow depths, the height of the tailings slope decreases over time or with increasing the number of loading cycles. The dissipation of pore pressure in the upstream side makes the associated tailings more resistant to earthquakes, while the tailings close to the slope surface slide along a failure plane in the silty layer or the interface. This eventually leads to the formation of terraces and scarps for the tailings left in place.

4 CONCLUDING REMARKS

This study characterized the failure mechanisms of upstream tailings impoundments subjected to seismic sequences based on centrifuge shaking table tests. The ejection of tailings, mudflows along the downstream slope of the starter dam and the

topographic features observed in real tailings impoundments after earthquake-induced failure are reproduced in the tests. The salient findings are summarized in the following.

For a sandy tailings slope with a laminar structure, the initial earthquakes may only lead to localized deformation near the silty layers at shallow depths, followed by lateral spreading of tailings between the silty layers at deeper locations. Those localized deformations can be attributed to the rapid buildup of pore pressure under silty layers. Although detachment and translocation of tailings protrusions may occur at the slope surface, the overall deformation of the tailings slope and the release of tailings are limited. The continuous buildup of pore pressure may lead to ejection of tailings during the subsequent earthquakes. After that, the excess pore pressure in the upstream side turns to dissipation, while the tailings near slope crest becomes liquefied and flow along the slope surface. The slope profile keeps changing with increasing the number of loading cycles until an extremely gentle slope with an angle of 1-2° emerges at the upper surface of the tailings impoundment. After that, the tailings at extremely shallow depths seem to be liquefied and then flow toward the downstream direction layer by layer, leading to the release of tailings. In addition, due to the continuous lateral spreading or sliding of tailings at deeper locations towards the downstream direction, the tailings eventually flow along the slope surface and then are released, which contributes to a significant increase in the release rate. Those results shed light on how failure occurs and how the tailings in the impoundments are released for a sandy tailings impoundment with a laminar structure subjected to seismic sequences.

5 ACKNOWLEDGEMENTS

This research was supported by National Natural Science Foundation of China (51809290) and Open Research Fund Program of State Key Laboratory of Hydroscience and Engineering (sklhse-2021-D-05). The authors are also grateful to reviewers for valuable comments.

6 REFERENCES

Adiansyah JS, Rosano M, Vink S, Keir G. A framework for a sustainable approach to mine tailings management: disposal strategies. J. Clean. Prod. 2015;108:1050-1062.

Agurto-Detzel H, Bianchi M, Assumpção M, et al. The tailings dam failure of 5 November 2015 in SE Brazil and its preceding seismic sequence, Geophys. Res. Lett., 2016, 43,4929–4936, doi:10.1002/ 2016GL069257.

Blight GE, Fourie AB Catastrophe revisited–disastrous flow failures of mine and municipal solid waste. Geotech. Geol. Eng. 2005,23(3):219-248.

Chen Q, Chen XH, and Zhu X, et al. Tailings dam design handbook. Metallurgical industry press. 2007. ISBN 8745786454. (in Chinese).

Dobry R, Alvares L. Seismic failures in Chilean tailings dams. J. Soil Mech. Found. Div. ASCE 1967,93(SM6):237-260.

Dong L, Deng S, Wang F. Some developments and new insights for environmental sustainability and disaster control of tailings dam. J. Clean. Prod. 2020. https://doi.org/10.1016/j.jclepro.2020.122270.

Fyfe WS. The environmental crisis: quantifying geosphere interactions. Science 1981;213(4503):105-110.

Hatje V, Pedreira RMA., de Rezende CE, Schettini CAF, de Souza GC, Marin DC, Hackspacher PC. The environmental impacts of one of the largest tailing dam failures worldwide. Sci. Rep. 2017,7(1):1-13.

Ishihara K, Ueno K, Yamada S, Yasuda S, Yoneoka T. Breach of a tailings dam in the 2011 earthquake in Japan. Soil Dyn. Earthq. Eng. 2015,68:3-22.

Ishihara K. Post-earthquake failure of a tailings dam due to liquefaction of pond deposit. Proccedings in International Conference on Case Histories in Geotechnical Engineering. 1984.

Jin J, Song C, Liang B, Chen Y, Su M. Dynamic characteristics of tailings reservoir under seismic load. Environ. Earth Sci. 2018,77(18):654.

Khanal A and Saygili G. Seismic Performance of Slopes Subjected to Earthquake Mainshock Aftershock Sequences. International Journal of Geological and Environmental Engineering, 2019, 13(5), 311 - 316.

Kim MK, Lee SH, Yun WC, Kim DS. Seismic behaviors of earth-core and concrete-faced rock-fill dams by dynamic centrifuge tests. Soil Dyn. Earthq. Eng. 2011,31:1579-1593.

Kokusho T, Kojima T. Mechanism for postliquefaction water film generation in layered sand. J. Geotech. Geoenviron. Eng. 2002,128(2): 129-137.

Kossoff D, Dubbin WE, Alfredsson M, Edwards SJ, Macklin MG, Hudson-Edwards KA. Mine tailings dams: characteristics, failure,S environmental impacts, and remediation[J]. Appl. Geochem. 2014,51:229-245.

Lottermoser B. Mine Wastes: Characterization, Treatment and Environmental Impacts. Springer, Berlin, Heidelberg, New York. 2007.

Madabhushi SSC, Haigh SK, Madabhushi GSP. LEAP-GWU-2015: Centrifuge and numerical modelling of slope liquefaction at the University of Cambridge. Soil Dyn. Earthq. Eng. 2018,113:671-681.

Owen JR, Kemp D, Lèbre É, Svobodova K, Murillo GP. Catastrophic tailings dam failures and disaster risk disclosure. Int. J. Disast. Risk Re. 2020;42:101361.

Santamarina JC, Torres-Cruz LA, Bachus RC. Why coal ash and tailings dam disasters occur. Science 2019,364(6440):526-528.

Schofield AN. Dynamic and earthquake geotechnical centrifuge modelling. Int. Conf. Recent Advances in Geotechnical Engineering and Soil Dynamics, 1981.

Shi JW, Fu ZZ, Guo WL. Investigation of geometric effects on three-dimensional tunnel deformation mechanisms due to basement excavation. Comput. Geotech. 2019,106:108-116.

Stewart D, Chen Y, and Kutter B. Experience with the Use of Methylcellulose as a Viscous Pore Fluid in Centrifuge Models. Geotechnical Testing Journal 21, no. 4 (1998): 365-369. https://doi.org/10.1520/GTJ11376J

Tanner DC, Buness H, Igel J, et al. Chapter 3 - Fault detection, Editor(s): Tanner DC and Brandes C, Understanding Faults, Elsevier, 2020, Pages 81-146, ISBN 9780128159859.

Troncoso JH, Vergara A, Avendaño A. Seismic Failure of Barahona Tailings Dam. Proceedings in 3rd Conference of the International Conference on Case Histories in Geotechnical Engineering. 1993.

Vergilio CdS, Lacerda D, Oliveira BCVd. et al. Metal concentrations and biological effects from one of the largest mining disasters in the world (Brumadinho, Minas Gerais, Brazil). Sci. Rep. 2020,10:5936. https://doi.org/10.1038/s41598-020-62700-w

Villavicencio G, Espinace R, Palma J, et al. Failures of sand tailings dams in a highly seismic country. Can. Geotech. J. 2014,51(4):449-464.

Zhang J. Study on tailing engineering geological character and stability of Li-West ditch tailing. Ph.D. Thesis. Changan University. 2006. (in Chinese)

Zhang XD, Zhang Z, Wei YQ, Liang JH, Hu J. Examining the seismic stress evolution in the face slab of concrete-faced rock-fill dams using dynamic centrifuge tests. Soil Dyn. Earthq. Eng. 2019,123:337-356.

Zobin VM. Chapter 19 - Seismic Activity at Dormant Volcanic Structures: A Problem of Failed Eruption, Editor(s): Zobin VM, Introduction to Volcanic Seismology (Third Edition), Elsevier, 2017, Pages 471-495, ISBN 9780444636317